



Structural and photoluminescence study of Mn doped ZnO nanostructures assisted by PVP

Ganga S. Kumar, Subhadra S. Nampoothiri, Melottil Niveetha, Krishna K.S.K. Arya, Palangadan Sajan®*

Research & Postgraduate Department of Physics, Devaswom Board Pampa College, Parumala, Pathanamthitta, 689626 Kerala, India

Received 6 June 2025; Received in revised form 1 September 2025; Accepted 12 September 2025

Abstract

The tuneable band gap properties of ZnO (II-VI semiconductor) make it an excellent host lattice phosphor for photonic and electroluminescent device applications. Here we report a simple and low-temperature chemical precipitation method (70 °C) to tune both morphology and optical emission of ZnO nanostructures using polyvinylpyrrolidone (PVP) and Mn doping. The effect of PVP addition on the structure of chemically synthesized hexagonal ZnO and Mn doped ZnO nanostructures was investigated. The morphology of the samples highlights the formation of nanorods in the pure ZnO while needle-like structure was obtained in the sample containing 22.8 wt.% of PVP. The optical and emission properties of the synthesized ZnO-based samples were also determined. The samples show semiconducting nature with a dual photoluminescence (PL) emission with distinct peaks observed at 411 and 563 nm. The morphology and PL emission showed tremendous change with the addition of 22.8 wt.% of PVP. Furthermore, the effect of Mn doping to the PVP modified ZnO samples was investigated. The blue PL emission at 437 nm in the Mn doped ZnO samples is due to both Mn doping and defects. The observed yellow emission at 564–573 nm region is attributed to the existence of defects such as singly ionised oxygen vacancies. This observed dual-emission behaviour with semiconducting bandgap holds great promise for various optoelectronic applications. Due to their distinct morphology, these unique needle-like structures can have significant potential applications.

Keywords: ZnO, nanoneedles, nanorods, chemical method, Mn doped ZnO, PVP assisted ZnO

I. Introduction

The size confined semiconductors, due to their significant optical and electrical capabilities, are valuable for developing multifunctional nano-scale devices in optoelectronics and electronics areas [1–3]. Being a unique semiconductor material, zinc oxide (ZnO) is widely used in electrical and photonic applications. Its wurtzite *n*-type crystal structure exhibits a substantial direct band gap of 3.37 eV at room temperature and a high room temperature exciton binding energy of 60 meV [4,5]. This property allows for excitonic transitions even at room temperature, having low threshold voltage for laser applications and high efficiency in radiative recombination for spontaneous emission. Additionally, ZnO wurtzite structure possesses strong pyro-

electric and piezoelectric capabilities, making it suitable for applications in mechanical actuators and piezoelectric sensors [6,7]. The wide properties of ZnO make it applications in the short wavelength range (UV, blue and green) sensors and also in information storage and optoelectronics [8]. Potential uses of ZnO nanoparticles include nano generators, solar cells, biosensors, photocatalysts, gas sensors, resistors and photodetectors [9,10]. Diverse properties of ZnO allow for a wide range of structural configurations and various techniques have been used to produce ZnO materials with different particle shapes, sizes and crystal structures. These nanomaterials have versatile applications in transistors, solar cells, biosensors and light emitting diodes due to their difference in shape, size and reactivity [11–13]. Zinc oxide is a commonly used metal oxide material with different applications like solar cells, varistors, lasers, LEDs, antireflection coatings, acoustic wave devices, cosmet-

e-mail: sajanp33@gmail.com

^{*}Corresponding authors: tel: +91 9946428564,

ics etc. [8,11]. The morphology and the aspect ratio play important role in manipulating their properties and hence their applications. It has been reported that ZnO with a hexagonal disc shape shows high photocatalytic activity [14,15]. The ZnO with flower-like morphology has shown much higher bio-activity and good adsorption properties [16,17]. Moreover, reports show that in the development of new functional materials, ZnO is having crucial role [18]. In this context tuning the morphology of ZnO is an important topic in the ZnO research.

Over the past years researchers have put effort in tuning the morphology of ZnO resulting in ZnO nanorods [17], plates, spheres, rings, flowers, dumbbell, nanotubes etc. [19]. Researchers developed several solution and vapour phase synthesis approaches like solgel process, solvothermal synthesis, flame spray pyrolysis, chemical vapour deposition, sonochemical technique, hydrothermal method, etc. for the fabrication of ZnO structures. In addition to these, several structure directing agents are used to control particle size as well as morphology of the materials. Several techniques have been developed to produce ZnO nanopowders, including organic precursors thermal decomposition, chemical vapour deposition, micro-emulsion, sol-gel, spray pyrolysis, electrodeposition, ultrasonic, microwave-assisted techniques, hydrothermal and precipitation methods [19-21]. Due to its simplicity and affordability among these methods, in the present study we used simple chemical precipitation method with the help of surfactant PVP (polyvinylpyrrolidone) for the synthesis of ZnO and Mn doped ZnO samples.

II. Experimental

For the preparation of pure ZnO sample, 8.78 g of zinc(II)-acetate dehydrate (98%, Spectrochem, India) was dissolved in 50 ml of deionized water and stirred for 5 min. Simultaneously 3.20 g of NaOH pellets was dissolved in 50 ml of deionized water and stirred for 5 min. After that, the two solutions were mixed drop-wise and stirred for 2 h 30 min at a temperature of 70 °C. The obtained suspension was filtered and washed several times with water and ethanol. The obtained precipitate was dried at 70 °C in a hot air oven for 2 h. The precipitate was ground to produce fine powder and used for analysis.

For the synthesis of the PVP capped ZnO, different amounts of polyvinylpyrrolidone (PVP) were added to zinc acetate (i.e. 1, 2 and 3 g, corresponding to 11.4, 22.8 and 34.2 wt.%) and the above procedure was repeated for all three powders. The obtained samples were denoted as: ZnO+PVP-1, ZnO+PVP-2 and ZnO+PVP-3.

In addition, the Mn doped PVP capped ZnO samples were prepared by adding different amounts of manganese(II)-acetate (98.5%, Loba Chemie, India) to the ZnO+PVP-2 mixture. To obtain Mn doped samples (denoted as ZnO+PVP-2+Mn-1 ZnO+PVP-2+Mn-3 and ZnO+PVP-2+Mn-5), 1, 3 and 5 wt.% of Mn(CH₃COO)₂ relative to the total mass of Zn(CH₃COO)₂ (corresponding to ~1.1, ~3.2 and ~5.3 at.% of Mn) was mixed with the ZnO+PVP-2 sample and the above synthesis procedure was repeated.

The obtained ZnO powders were analysed using X-ray diffraction (XRD), diffuse reflectance spectroscopy

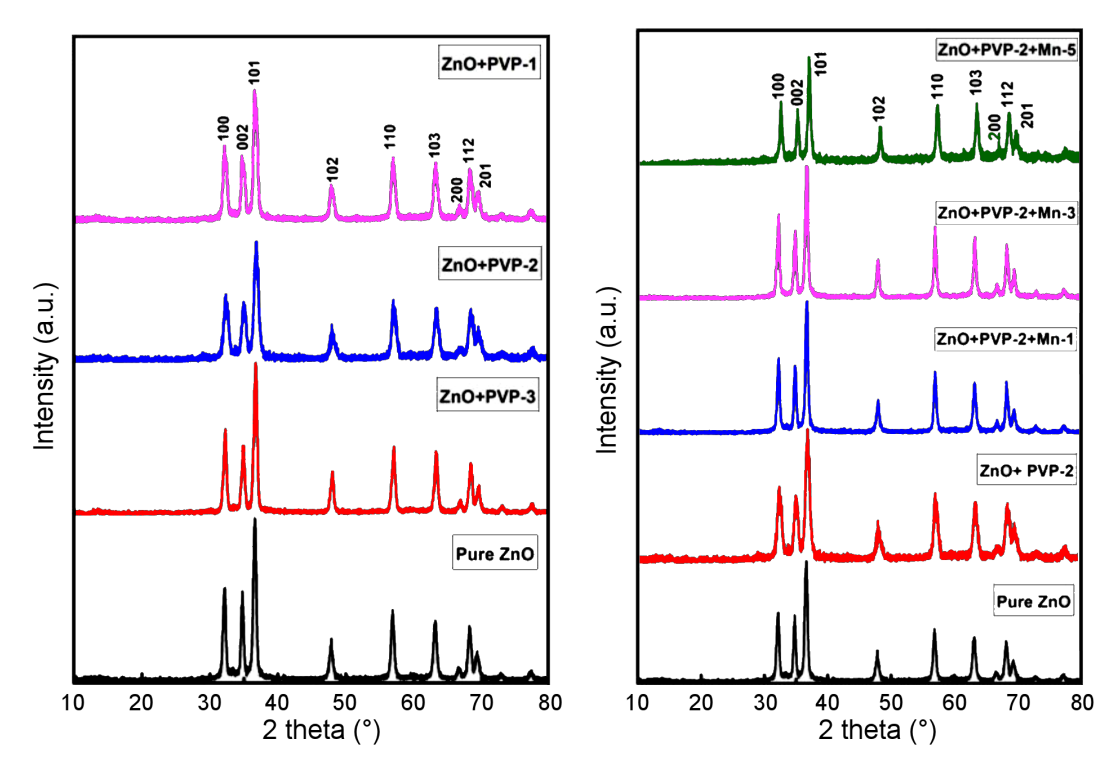


Figure 1. X-ray diffraction (XRD) patterns of the pure ZnO, PVP assisted ZnO and PVP assisted Mn doped ZnO samples synthesized at a temperatures of 70 °C via simple chemical precipitation method

Table 1. Lattice parameters and crystallite sizes of the pure ZnO, PVP assisted ZnO and PVP assisted Mn doped ZnO samples synthesized at $70\,^{\circ}\mathrm{C}$ via simple chemical precipitation method

Samples	Lattice parameter		Crystallite size
Samples	a [Å]	c [Å]	[nm]
Pure ZnO	3.21	5.18	17.7
ZnO+PVP-1	3.20	5.21	16.2
ZnO+PVP-2	3.19	5.16	11.5
ZnO+PVP-3	3.21	5.23	13.1
ZnO+PVP-2+Mn-1	3.20	5.18	19.46
ZnO+PVP-2+Mn-3	3.22	5.13	18.73
ZnO+PVP-2+Mn-5	3.17	5.18	17.12

(DRS), Fourier-transform infrared spectroscopy (FTIR) and field emission scanning electron microscopy (FE-SEM). The morphology of the samples was examined with a Carl Zeiss Sigma FESEM. XRD patterns of the synthesized ZnO-based powders were recorded using a Rigaku tabletop X-ray diffractometer with CuK α radiation ($\lambda = 1.5418$ Å) within the 2θ range of 10–90°. The diffused reflectance spectra (DRS) were measured using a JASCO V-570 spectrometer and the FTIR measurements were conducted using a Shimadzu FTIR spectrometer with the KBr pellet method.

III. Results and discussion

3.1. XRD studies

XRD patterns of the pure ZnO, PVP modified ZnO and Mn doped PVP-ZnO samples synthesized at 70 °C via simple chemical precipitation method were shown in Fig. 1. The observed peaks in all the samples can be indexed to ICDD card No. 36-1451 which shows the growth of the hexagonal structure of ZnO while no peaks of a secondary phase were observed. Mn²⁺ ions

are incorporated in ZnO structure, since there is similarity between ionic radii of $\mathrm{Mn^{2+}}$ (0.80 Å) and $\mathrm{Zn^{2+}}$ (0.74 Å). The lattice parameters and crystalline sizes calculated from XRD data, shown in Table 1, are in good agreement with the reported values in the literature [5]. The crystallite sizes show a slight decrease with the addition of PVP, while the increase with Mn doping suggests that Mn controls the crystal growth [22].

3.2. SEM studies

Figure 2a shows the pure ZnO sample having particles with nanorod shape. However, the samples with PVP have characteristic needle-like structure. The observed needle-like structured ZnO (Fig. 2c) consists of needle particles having the lengths of 80–90 nm. The powders ZnO+PVP-1 (Fig. 2b) and ZnO+PVP-3 (Fig. 2d) consist of nanosized particles which are agglomerated. However, it seems that the addition of 2 g PVP to the growth medium leads to the sample (ZnO+PVP-2) being less agglomerated (Fig 2c). It is reported that PVP provides efficient stabilization at an optimal concentration, which enhances the surface morphology without

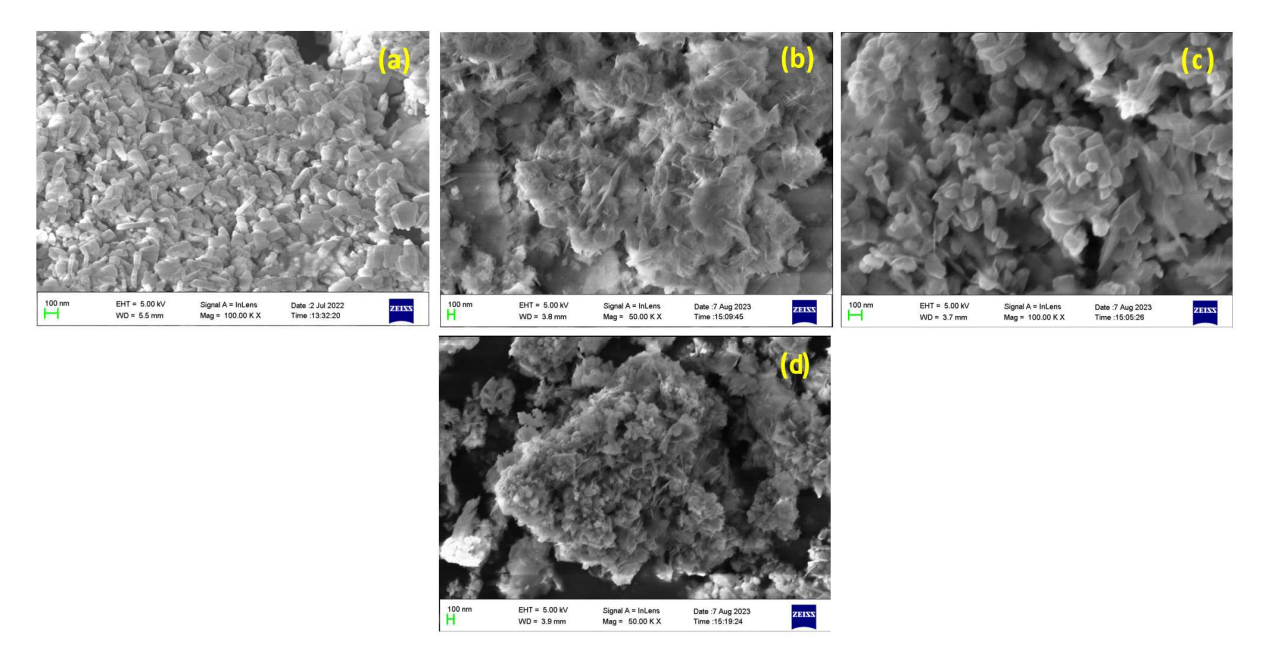


Figure 2. FESEM image of pure ZnO (a), ZnO+PVP-1(b), ZnO+PVP-2 (c) and ZnO+PVP-3 (d) synthesized at $70\,^{\circ}$ C via simple chemical precipitation method

Figure 3. SEM images of ZnO+PVP-2+Mn-1 (a), ZnO+PVP-2+Mn-3 (b) and ZnO+PVP-2+Mn-5 (c) grown at $70\,^{\circ}$ C via simple chemical precipitation method

overly restricting the crystallite growth [23]. This is confirmed by the presented results and the fact that the optimal concentration is 2 g of PVP used in the sample ZnO+PVP-2.

The surface morphologies of the Mn doped PVP-ZnO samples are shown in Fig. 3. The reduced agglomeration in the Mn doped ZnO samples can be seen together with inhibited formation of needle-like particles (Fig. 2c) [24].

3.3. FTIR analysis

The FTIR analysis (Fig. 4) further supports the structural characterization of the prepared ZnO-based samples. The absorption bands observed at 706 and 836 cm⁻¹ are attributed to Zn–O vibrational modes. The peaks observed around 2400 cm⁻¹ are assigned to the presence of atmospheric CO₂ [25]. For the PVP-modified samples, peaks at 1040–1498 cm⁻¹ correspond to the C–N stretching bond of PVP. The Mn doped sam-

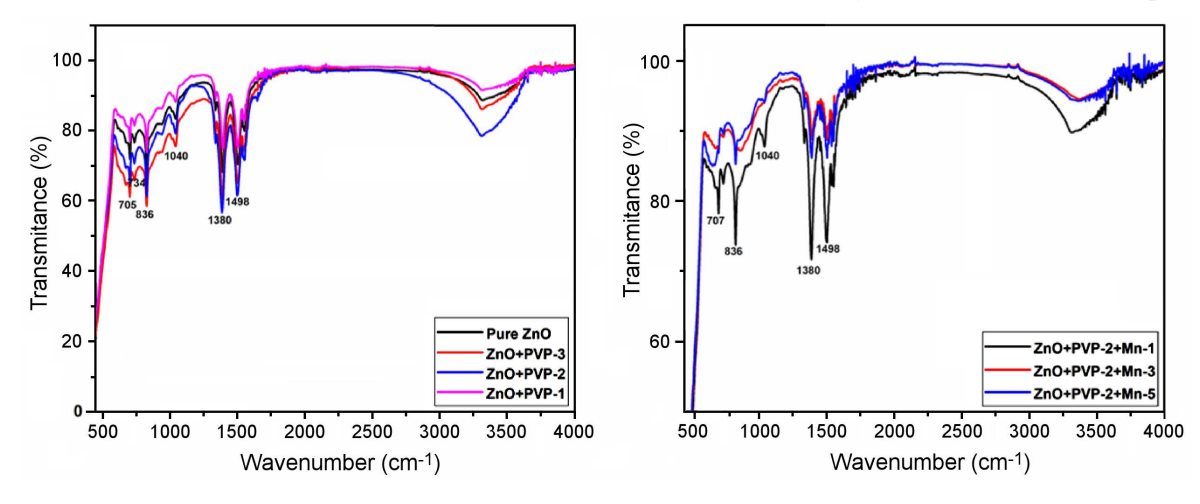


Figure 4. FTIR spectra of the pure ZnO, PVP assisted ZnO and PVP assisted Mn doped ZnO samples synthesized at $70\,^{\circ}\mathrm{C}$ via simple chemical precipitation method

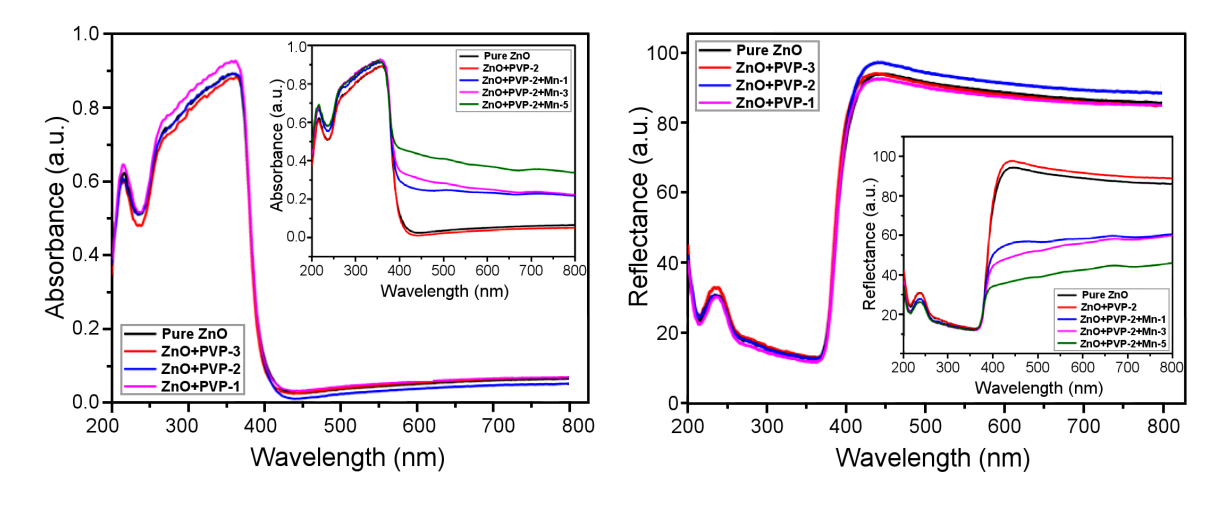


Figure 5. The absorbance (a) and reflectance (b) spectra of the pure ZnO, PVP assisted ZnO and PVP assisted Mn doped ZnO samples synthesized at 70 °C via simple chemical precipitation method

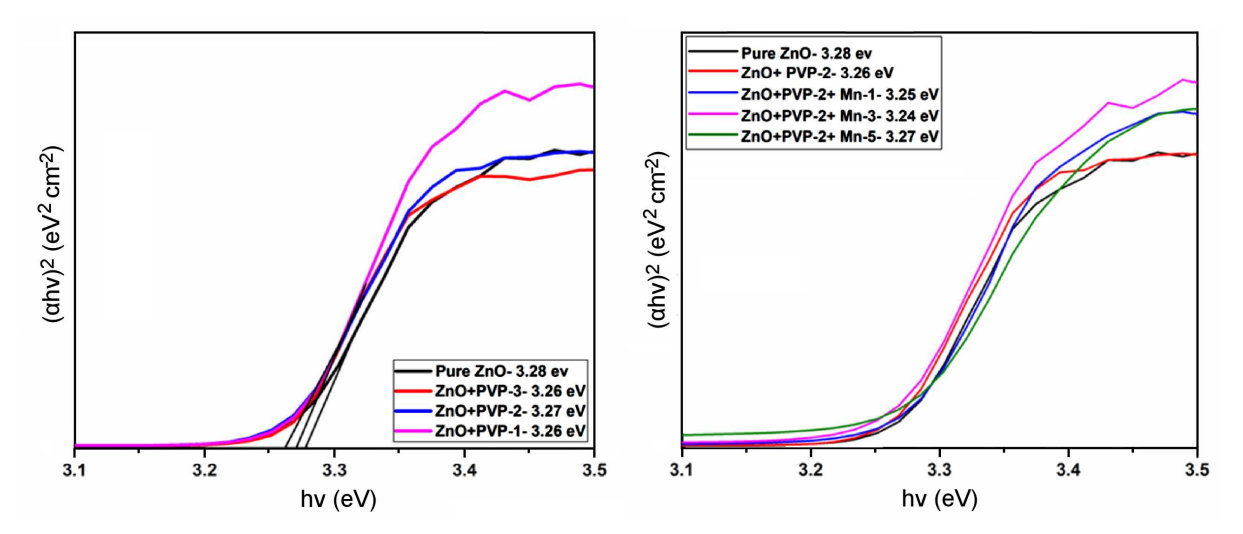


Figure 6. The Tauc plot of the pure ZnO, PVP assisted ZnO and PVP assisted Mn doped ZnO samples synthesized at 70 °C via simple chemical precipitation method

ples show small peaks at 662 and 836 cm⁻¹ indicating M–O stretching bond [25].

3.4. Optical properties

The optical properties of the synthesized sample are depicted with the absorbance (Fig. 5a) and the reflectance spectra (Fig. 5b). All the samples show an absorption edge in the region 380–420 nm (Fig. 5a). The slight variation between the absorption spectra of the Mn doped ZnO samples is attributed to the formed defects. The band gaps of the prepared samples were calculated using the Kubelka-Munk relation from the reflectance spectra (Fig. 5b) and shown in Fig. 6 and Table 2. The slight decrease in band gap with Mn addition can be related to the introduced defect levels within the band gap. This effect is ascribed to the *s-d* and *p-d* exchange interactions between the dopant and the host material [26].

The photoluminescence (PL) spectra of the samples with an excitation of 325 nm are shown in Fig. 7. The samples show broad emission in the region 520–620 nm centred at 563 nm with an excitation of 325 nm. The ob-

Table 2. Band gap of the pure ZnO, PVP assisted ZnO and PVP assisted Mn doped ZnO samples synthesized at 70 °C via simple chemical precipitation method

Samples	Band gap [eV]	
Pure ZnO	3.28	
ZnO+PVP-1	3.26	
ZnO+PVP-2	3.27	
ZnO+PVP-3	3.26	
ZnO+PVP-2+Mn-1	3.25	
ZnO+PVP-2+Mn-3	3.24	
ZnO+PVP-2+Mn-5	3.27	

served yellow emission at 564–573 nm is attributed to the existence of defects such as singly ionized oxygen vacancies as reported in the literature [27]. The addition of PVP to ZnO nanoparticles enhanced their photoluminescence properties which are pronounced for the ZnO+PVP-2 sample. This enhancement is attributed to the passivization of surface defects by PVP, which then reduced non-radiative recombination centres. This reduction, in turn, helps in radiative recombination, re-

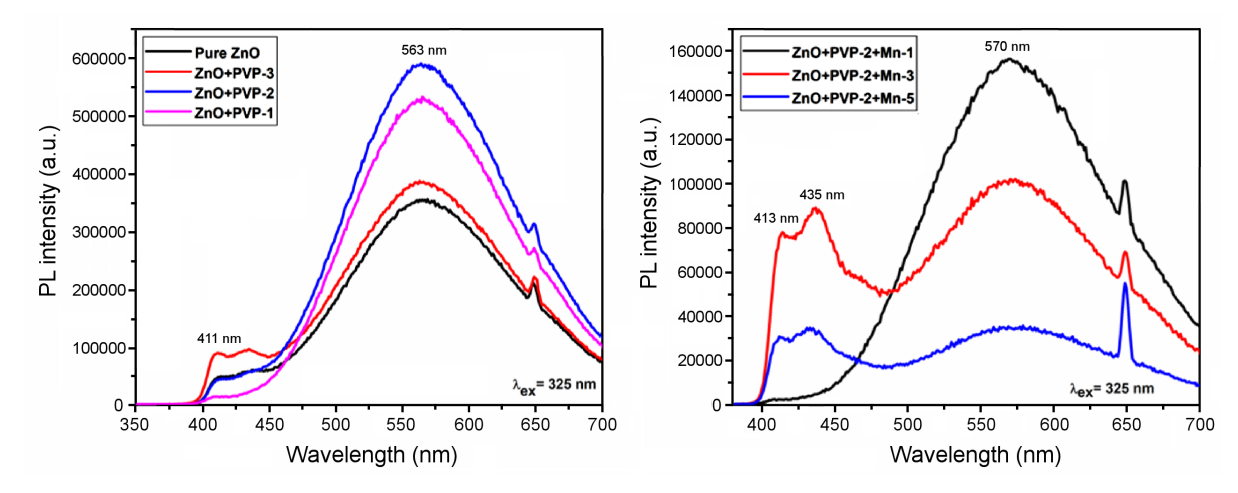


Figure 7. The room temperature PL spectra of the pure ZnO, PVP assisted ZnO and PVP assisted Mn doped ZnO samples synthesized at 70 °C via simple chemical precipitation method

sulting in stronger photoluminescence emissions. [23]. Tachikawa et al. [27] reported that adding PVP to ZnO nanoparticles solutions after synthesis resulted in a 27% increase in the fluorescence intensity compared to samples without PVP addition. For the incorporation of Mn²⁺ ion into the ZnO lattice, it is important to consider their respective ionic radii. The ionic radius of Zn²⁺ is approximately 0.74 Å, while that of Mn²⁺ is about 0.80 Å [28–30]. A small difference in size ($\sim 0.06 \text{ Å}$) allows Mn²⁺ to substitute Zn²⁺ in the wurtzite ZnO structure without significantly distorting the lattice. This substitution is favourable and widely reported in the literature for Mn doping concentrations within a few atomic percent [28–30]. Furthermore, it is reported that such substitution may induce structural strain and facilitate the formation of intrinsic defects, particularly oxygen vacancies [28–30]. These defects are known to contribute to the observed yellow photoluminescence in the 564–573 nm range, supporting the presence of singly ionized oxygen vacancies as a dominant recombination centre in Mn-doped ZnO samples [28-30]. In the PL spectra of the Mn doped ZnO samples one can observe dual emission with an excitation of 325 nm. The sample shows blue emission at 437 nm due to both the Mn doping and defects in ZnO. The observed vellow emission at 564-573 nm is attributed to the existence of defects such as singly ionised oxygen vacancies as reported in the literature [24,31]. There is a decrease in the intensity of PL emission with increase in Mn concentration which indicates the increase of nonradiative recombination process [24,31]. The structural defects or vacancies or both of them are attributed with the emission of different colours in the PL spectrum. In ZnO the structural defects are mainly due to the interstitial zinc and interstitial oxygen [24,31]. The blue peak can be due to the recombination of free exciton through an excitonexciton collision process or the transition of electron between the Zn; donor level and top level of valence band [24,31].

IV. Conclusions

In summary, we have successfully synthesized pure ZnO, PVP modified ZnO and Mn doped ZnO-PVP nanostructures using more cost-effective, simple lowtemperature chemical precipitation method at 70 °C. All the samples show the hexagonal wurtzite structure as confirmed by XRD. The surface morphology of the ZnO-based samples shows the growth of needle like structure with the addition of PVP. The addition of PVP to the growth medium modified the morphology leading to the formation of needle-like structures, in contrast to the more commonly observed nanorod structures in the pure and Mn doped ZnO materials. The photoluminescence has increased with the addition of PVP, showing emission in the region 520-620 nm range centred at 563 nm. The samples show PL dual emission in the blue region around 411, 413, 435 nm and yellow region at 563 and 570 nm. The observed yellow emission is attributed to the existence of defects such as singly ionized oxygen vacancies. All the samples show semiconducting band gap nature and the yellow emission from the samples along with the blue emission can be used as potential material in the field of semiconductor devices and photonic applications. We have optimized the reaction condition to synthesize the ZnO nanorods and needles which can be a good candidate for the photonic applications.

Acknowledgement: Authors thanks Department of Physics, Cochin University of Science and Technology (CUSAT), Kochi, Kerala for the FESEM Analysis and Post-Graduate Department of Chemistry, Devaswom Board Pampa College, Parumala, Kerala, for providing lab facility.

References

- X. Yan, Y. Li, X. Zhang, "Semiconductor nanowire heterodimensional structures toward advanced optoelectronic devices", *Nanoscale Horizons*, 10 (2025) 56–77.
- 2. J. Mondal, R. Lamba, Y. Yukta, R. Yadav, R. Kumar, B. Pani, B. Singh, "Advancements in semiconductor quantum dots: Expanding frontiers in optoelectronics, analytical sensing, biomedicine, and catalysis", *J. Mater. Chem. C*, **12** (2024) 10330–10389.
- 3. S. Aftab, G. Koyyada, M. Mukhtar, H.H. Hegazy, J.H. Kim, "From energy to light: Advancements in perovskite quantum dots for optoelectronics", *J. Mater. Chem. C*, **12** (2024) 17789–17801.
- J.G. Lu, Z. Fan, D. Wang, P.-C. Chang, "Electrical and optical properties of ZnO nanowires", *Proceedings of SPIE*, 5648 (2004) 260–268.
- R. Vinod, P. Sajan, S.R. Achary, C. Martinez Tomas, V. Muñoz-Sanjosé, M. Junaid Bushiri, "Enhanced UV emission from ZnO nanoflowers synthesized by the hydrothermal process", *J. Phys. D: Appl. Phys.*, 45 (2012) 425103.
- R. Matsuzaki, H. Soma, K. Fukuoka, K. Kodama, A. Asahara, T. Suemoto, Y. Adachi, T. Uchino, "Purely excitonic lasing in ZnO microcrystals: Temperature-induced transition between exciton-exciton and exciton-electron scattering", *Phys. Rev. B*, 96 [12] (2017) 125306.
- C.-C. Hsiao, S.-Y. Yu, "Improved response of ZnO films for pyroelectric devices", *Sensors*, 12 [12] (2012) 17007– 17022.
- 8. G. Li, B. Cheng, H. Zhang, X. Zhu, D. Yang, "Progress in UV photodetectors based on ZnO nanomaterials: A review of the detection mechanisms and their improvement", *Nanomaterials*, **15** [9] (2025) 644.
- 9. A. Wibowo, M.A. Marsudi, M.I. Amal, M.B. Ananda, R. Stephanie, H. Ardy, L.J. Diguna, "ZnO nanostructured materials for emerging solar cell applications", *RSC Advances*, **10** [70] (2020) 42838–42859.
- 10. M.S. Krishna, S. Singh, M. Batool, H.M. Fahmy, K. Seku, A.E. Shalan, S. Lanceros-Mendez, M.N. Zafar, "A review on 2D-ZnO nanostructure based biosensors: From materials to devices", *Mater. Adv.*, **4** (2023) 320–354.
- 11. Ü. Özgür, Y.I. Alivov, C. Liu, A. Teke, M.A. Reshchikov, S. Doğan, V. Avrutin, S.-J. Cho, H. Morkoç, "A comprehensive review of ZnO materials and devices", *J. Appl.*

- Phys., 98 [4] (2005) 041301.
- 12. Z.L. Wang, "Zinc oxide nanostructures: growth, properties and applications", *J. Phys. Condens. Matter*, **16** [25] (2004) R829–R858.
- Y. Zhang, T.R. Nayak, H. Hong, W. Cai, "Biomedical applications of zinc oxide nanomaterials", *Curr. Mol. Med.*, 13 [10] (2013) 1633–1645.
- 14. S. Baruah, J. Dutta, "Hydrothermal growth of ZnO nanostructures", *Sci. Technol. Adv. Mater.*, **10** (2009) 013001.
- M. Maruthupandy, T. Muneeswaran, G. Chackaravarthi, T. Vennila, M. Anand, W.-S. Cho, F. Quero, "Development of hexagonal ZnO nanodisks for potential catalytic reduction of p-nitrophenol", *Mater. Chem. Phys.*, 285 (2022) 126145.
- L. Fang, K. Huang, B. Zhang, Y. Liu, Q. Zhang, "A label-free electrochemistry biosensor based on flower-like 3-dimensional ZnO superstructures for detection of DNA arrays", New J. Chem., 38 [12] (2014) 5918–5924.
- 17. R. Vinayagam, S. Pai, G. Murugesan, T. Varadavenkatesan, R. Selvaraj, "Synthesis of photocatalytic zinc oxide nanoflowers using *Peltophorum pterocarpum* pod extract and their characterization", *Appl. Nanosci.*, **13** [1] (2023) 847–857.
- 18. M.A. Borysiewicz, "ZnO as a functional material: A review", *Crystals*, **9** [10] (2019) 505.
- 19. P. Ma, Y. Jie, G.Y. Jin, X.L. Xu, Z.Y. Ren, H.M. Fan, "Formation of thin tubular ZnO nanostructure through spontaneously formed porous Zn/ZnO nanoparticles", *Micro Nano Lett.*, **8** [5] (2013) 267–270.
- H. Neelamkodan, U. Megha, M.P. Binitha, "Enhanced green luminescence properties of Cu doped ZnO nanoflowers and their improved antibacterial activities", *Pro*cess. Appl. Ceram., 17 [1] (2023) 81–90.
- K.M. Mohamed, J. John Benitto, J. Judith Vijaya, M. Bououdina, "Recent advances in ZnO-based nanostructures for the photocatalytic degradation of hazardous, non-biodegradable medicines", Crystals, 13 [2] (2023) 329.
- J.-F. Yan, T.-G. You, Z.-Y. Zhang, J.-X. Tian, J.-N. Yun, W. Zhao, "Effect of Mn-doping on the growth mechanism and electromagnetic properties of chrysanthemum-like

- ZnO nanowire clusters", *Chin. Phys. B*, **20** [4] (2011) 048102.
- 23. H.M. Kamari, N.M. Al-Hada, E. Saion, A.H. Shaari, Z.A. Talib, M.H. Flaifel, A.A.A. Ahmed, "Calcined solution-based PVP influence on ZnO semiconductor nanoparticle properties", *Crystals*, 7 [2] (2017) 2.
- S.A. Ahmed, "Structural, optical, and magnetic properties of Mn-doped ZnO samples", *Results Phys.*, 7 (2017) 604– 610
- 25. D. Ghica, I.D. Vlaicu, M. Stefan, S.V. Nistor, "On the agent role of Mn²⁺ in redirecting the synthesis of Zn(OH)₂ towards nano-ZnO with variable morphology", *RSC Adv.*, **6** (2016) 106732–106741.
- W.H. Shah, A. Alam, H. Javed, K. Rashid, A. Ali, L. Ali, A. Safeen, M.R. Ali, N. Imran, M. Sohail, G. Chambashi, "Tuning of the band gap and dielectric loss factor by Mn doping of Zn_{1-x}Mn_xO nanoparticles", *Sci. Rep.*, 13 (2023) 8646.
- S. Tachikawa, A. Noguchi, T. Tsuge, M. Hara, O. Odawara, H. Wada, "Optical properties of ZnO nanoparticles capped with polymers", *Materials*, 4 [6] (2011) 1132–1143.
- S.D. Senol, B. Yalçin, E. Ozugurlu, L. Arda, "Structure, microstructure, optical and photocatalytic properties of Mn-doped ZnO nanoparticles", *Mater. Res. Express*, 7 [1] (2020) 015079.
- F. Lekoui, R. Amrani, W. Filali, E. Garoudja, L. Sebih, I.E. Bakouk, H. Akkari, S. Hassani, N. Saoula, S. Oussalah, H. Albalawi, N. Alwadai, M. Henini, "Investigation of the effects of thermal annealing on the structural, morphological and optical properties of nanostructured Mn doped ZnO thin films", Opt. Mater., 118 (2021) 111236.
- 30. A. Janotti, C.G. Van de Walle, "Fundamentals of zinc oxide as a semiconductor", *Rep. Prog. Phys.*, **72** (2009) 126501.
- I. Aadnan, O. Zegaoui, A. El Mragui, I. Daou, H. Moussout, J.C.G. Esteves da Silva, "Structural, optical and photocatalytic properties of Mn doped ZnO nanoparticles used as photocatalysts for azo-dye degradation under visible light", Catalysts, 12 [11] (2022) 1382.